European Journal of Radiology 128 (2020) 109031

Contents lists available at ScienceDirect

European Journal of Radiology

journal homepage: www.elsevier.com/locate/ejrad

IDH1 mutation prediction using MR-based radiomics in glioblastoma: comparison between manual and fully automated deep learning-based approach of tumor segmentation

Yangsean Choi[1], Yoonho Nam[1,2], Youn Soo Lee[3], Jiwoong Kim[1], Kook-Jin Ahn[1,*], Jinhee Jang[1], Na-Young Shin[1], Bum-Soo Kim[1], Sin-Soo Jeon[4]

[1] Department of Radiology, Seoul St. Mary's Hospital, College of Medicine, The Catholic University of Korea, Seoul, Republic of Korea
[2] Division of Biomedical Engineering, Hankuk University of Foreign Studies, Yongin-Si, Gyeonggi-do, Republic of Korea
[3] Department of Hospital Pathology, Seoul St. Mary's Hospital, College of Medicine, The Catholic University of Korea, Seoul, Republic of Korea
[4] Department of Neurosurgery, Seoul St. Mary's Hospital, College of Medicine, The Catholic University of Korea, Seoul, Republic of Korea

ARTICLE INFO

Keywords:
glioblastoma
isocitrate dehydrogenase
magnetic resonance imaging
machine learning
sensitivity and specificity

ABSTRACT

Purpose: This study aimed to determine whether MR-based radiomics of glioblastoma can predict the isocitrate dehydrogenase-1 (IDH1) mutation status and compare predictive performances between manual and fully automatic deep-learning segmentations.

Method: Forty-five glioblastoma patients with pretreatment T2-weighted MRIs were retrospectively evaluated. Manual segmentations of glioblastoma and peri-tumoral edema were trained via a deep neural network (V-Net). An independent external cohort of 137 glioblastoma patients from the Cancer Imaging Archive was also included (test set 1, n = 46; test set 2, n = 91). Test set 1—without known IDH1 status—was used to calculate dice similarity coefficients (DSC) between the two segmentation methods (manual & V-Net). From test set 2, all-relevant radiomic features were selected via a random forest-based wrapper algorithm for IDH1 prediction. Receiver operating characteristics (ROC) curves with areas under the curve (AUC) were plotted as performance metrics for both methods.

Results: Among 136 patients (45 and 91 patients from our institution and test set 2, respectively), 17 patients (11.2 %) had IDH1 mutations. The mean DSC of test set 1 was 0.78 ± 0.14 (range, 0.34 − 0.94). A subset of 9 all-relevant features (8.4 %, 9/107) was selected. V-Net segmentation of the test set 2 yielded similar performance in predicting IDH1 mutation as compared to manual segmentation (V-Net AUC = 0.86 vs. manual AUC = 0.90). The optimal cut-point threshold of AUC yielded 86.8 % accuracy for manual segmentation and 75.8 % for V-Net segmentation.

Conclusions: V-Net showed robust segmentation capability of glioblastoma on T2-weighted MRI. All-relevant radiomics features from both segmentation methods yielded a similar performance in IDH1 prediction.

1. Introduction

Glioblastoma is the most common primary malignant brain tumor that is known for its dismal prognosis (average survival: approximately 1 year) [1]. Histologically, de novo glioblastoma shows the presence of wild-type isocitrate dehydrogenase-1 (IDH1). Secondary glioblastoma arising from lower grade gliomas has mutant IDH1 and occurs in about 12 % of glioblastomas [2]. The mutant IDH1 status indicates a better prognosis [3,4]. As a result, assessing the status of the IDH1 mutation—a well-known prognostic biomarker—would help in prognostication of patients prior to histologic confirmation.

To quantitatively assess glioblastoma on MRI, appropriate tumor segmentation is required, which is often time-consuming, labor-intensive, and subjective. Convolutional neural network (CNN)-based image segmentation has gained popularity for its applications in segmenting various anatomical structures and lesions including coronary

Abbreviations: 3D, three-dimensional; ROC, receiver operating characteristics; AUC, area under the curve; CNN, convolutional neural network; DSC, dice similarity coefficient; IDH1, isocitrate dehydrogenase-1; TCIA, The Cancer Imaging Archive; TCGA, The Cancer Genome Atlas; T2WI, T2-weighted image

* Corresponding author at: Department of Radiology, Seoul St. Mary's Hospital, College of Medicine, The Catholic University of Korea, 222 Banpo-daero, Seocho-gu, Seoul 06591, Republic of Korea.
E-mail address: ahn-kj@catholic.ac.kr (K.-J. Ahn).

https://doi.org/10.1016/j.ejrad.2020.109031
Received 18 December 2019; Received in revised form 9 April 2020; Accepted 19 April 2020

arteries [5], abdominal organs [6,7], proximal femur [8], prostate [9–11], and brain tumors [12,13]. Most approaches of CNN-based image segmentations have focused on processing two-dimensional images while most medical images comprise three-dimensional (3D) volumes. V-Net is a CNN that implements 3D convolutional layers for medical image segmentation. Residual connection and volumetric dice metric are unique characteristics of V-Net that distinguish it from other computerized methods. Overall, V-Net can analyze fine details of organs of various shapes and textures, thus making it a generalized tool for medical segmentation [14]. We hypothesized that V-Net would be capable of segmenting glioblastoma and peritumoral edema on pretreatment T2-weighted MRI, as a result of which the radiomic features from these segmentations would reliably predict the IDH1 mutation status.

In this study, we aimed to apply MR-based radiomics to extract features that would differentiate IDH1 mutant glioblastoma from wild-type IDH1. In doing so, we attempted to segment tumors via a fully automated CNN method named V-Net and compare its performance to that of manual segmentations.

2. Material and Methods

2.1. Patient Selection

The institutional review board of our institution approved this retrospective study and waived informed consent. The inclusion criteria of the patients were: (1) pathologically confirmed WHO Grade IV glioblastoma; (2) available pretreatment brain MRI with T2-weighted images (T2WI); (3) known IDH1 status; and (4) no prior history of surgery or radiotherapy. Two independent patient cohorts were included. First, a retrospective review of electronic medical records in our institution from March 2009 to April 2018 yielded 45 eligible patients. The Cancer Imaging Archive (TCIA) and The Cancer Genome Atlas (TCGA), an open-source imaging and genetic repository, respectively [15], were reviewed to include two additional test sets: test set 1 (n = 46, without known IDH1 status) and test set 2 (n = 91). Glioblastomas patients in both test sets were selected using the above inclusion criteria, except for test set 1 patients whose IDH1 status was not known. The flow diagram of training V-Net and analyzing two test sets is depicted in Fig. 1.

2.2. MRI Acquisition Protocol

Two different 3.0-T MR scanners were used to acquire the images: Magnetom Verio (Siemens Healthineers, Erlangen, Germany; 12-channel phased-array coil) and Ingenia (Philips Healthcare, Best, the Netherlands; 32-channel phased-array coil). The acquisition parameters for both scanners were: axial T2WI (repetition time = 3000–5500 ms; echo time = 80–95 ms; flip angle = 150°; field of view = 210 × 210 mm; acquired matrix = 448 × 358; number of excitations = 1; echo train length = 17; section thickness = 4 − 5 mm). For the TCIA cohort, MR images were obtained with either a 1.5-T (n = 66) or 3.0-T (n = 25) scanner. The acquisition parameters were axial T2WI (repetition time = 3000–5500 ms; echo time = 80–105 ms; flip angle = 90°; field of view = 200 × 200–240 × 240 mm; acquired matrix = 256 × 192–256 × 224; number of excitations = 1–2; echo train length = 8; section thickness = 5 mm).

2.3. IDH1 Sequence Analyses

At our institution, the QIAamp DNA Mini Kit (QIAGEN, Hilden, Germany) was used to extract genomic DNA from 10 μm thick sections of 10 % neutral formalin-fixed paraffin-embedded tissue blocks. The entire coding sequence of exon 4 of the IDH1 gene as well as codon 132 was acquired by overlapping polymerase chain reaction amplification, which was performed in 20 μL containing 100 ng of template DNA, 10 μL PCR buffer, 0.25 mM dNTPs, 10 pmol primers, and 1.25 U Taq DNA polymerase (iNtRON, Seoul, Korea). The following primer sequences were used: forward, 50-CGGTCTTCAGAGAAGCCATT-30 and reverse primer, 50-GCAAAATCACATTATTGCCAAC-30. The products of PCR were electrophoresed on 2 % agarose gels and purified with a QIAquick PCR purification kit (QIAGEN, Hilden, Germany). The BigDye Terminator v1.1 kit (Applied Biosystems, Foster City, CA, USA) on an ABI 313091 genetic analyzer (Applied Biosystems) was used for bidirectional sequencing. For the TCIA/TGCA cohort, median normalized messenger RNA expression data (Affymetrix HG U133A array) was obtained from the TCGA Data portal [15].

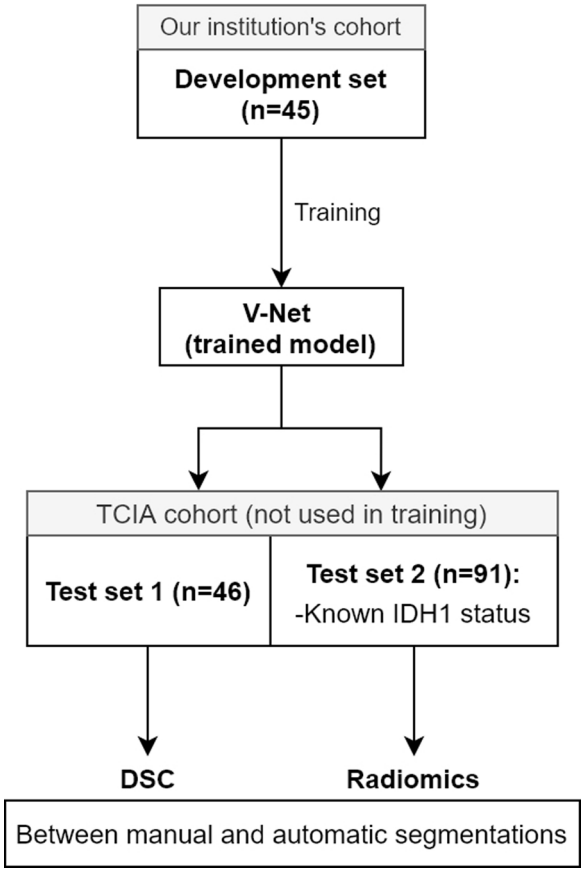

Fig. 1. Flowchart showing grouping of cohorts into development and test sets with subsequent analyses.

2.4. Manual Segmentation

On T2WI, ROI encompassing the entire tumor (i.e. enhancing and non-enhancing portion including necrosis) and peri-tumoral edema were drawn semi-automatically on each slice by a radiologist with 6 years of experience in neuroradiology (Y.C.) using a 3D Slicer [16] (www.slicer.org) (Supplementary Fig. 1). The segmented images were further reviewed and confirmed by another radiologist with 20 years of experience in neuroradiology (K.J.A.). Both radiologists were blinded to the patients' clinical information. Manual segmentations were drawn for patients from our institution with known IDH1 status (n = 45) and in both test sets of the TCIA cohort (test set 1, n = 46; test set 2, n = 91). For dice similarity coefficient (DSC) calculation, test set 1 was used as reference to which the output of automatic segmentation could be compared (Fig. 1).

2.5. Automatic Segmentation via V-Net

The application of the V-Net [14] was primarily based on previous

Table 1
Baseline characteristics of study cohorts.

Clinical characteristics	Our institution (n = 45) (development set)	TCIA/TCGA (n = 91) (test set)	*P* value
Sex, n (%)			
Male	24 (53.3 %)	53 (58.2 %)	0.719
Female	21 (46.7 %)	38 (41.8 %)	
Age, mean ± SD	58.7 ± 12.9	58.6 ± 15.2	0.971
Tumor location, n (%)			0.183
Frontal	14 (31.1 %)	23 (25.3 %)	
Occipital	3 (6.7 %)	4 (4.4 %)	
Parietal	13 (28.9 %)	27 (29.7 %)	
Temporal	9 (20 %)	32 (35.2 %)	
Midline	4 (8.9 %)	5 (5.5 %)	
Cerebellum	2 (4.4 %)	0 (0%)	
IDH1 status, n (%)			
Wild-type	38 (84.4 %)	83 (91.2 %)	0.371
Mutated	7 (15.6 %)	8 (8.8 %)	

TCIA = the cancer imaging archive, SD = standard deviation, IDH1 = isocitrate dehydrogenase-1.

experiments on a GitHub repository (https://github.com/mattmacy/vnet.pytorch). The V-net is similar to U-net [14,17], except that it uses 3D input and output and convolution with a stride of factor 2 instead of max-pooling. The V-net structure was used with modification of dice loss function which was used as:

$$\frac{[2 \times sum(< ground\ truth > < prediction >)]}{[sum(< ground\ truth >^2) + sum(< prediction >^2) + 0.0001]}$$

The ADAM optimizer was used to update the network parameters. The learning rate, number of epochs, and batch size were 0.001, 128, and 4, respectively. The training and tests were performed on a single GPU (NVIDIA Geforce GTX 2080 ti) using PyTorch v1.0. The model training time was approximately 2 h; the inference time for the test data segmentation was about 0.1 s per patient.

For all T2WI data, a ranged (minimum = 0, maximum = 1) intensity normalization was performed and interpolated to 1.5 mm isotropic space before segmentation and radiomics analysis. Firstly, for reference segmentations, 45 manually segmented T2WI patients from our institution were used to train the V-Net architectures, wherein 5 randomly selected patients' T2WI were used solely for network structure and hyperparameter optimization purposes. The trained V-net model was used to test the 46 unsegmented T2WI in test set 1. Finally, this V-Net model was used to test the 91 T2WI in test set 2 to obtain tumor segmentations. Both test sets were not used in the training process to avoid overfitting.

2.6. Evaluation of Segmentation Accuracy

Test set 1 was used for DSC calculation. The segmented volumes from manual and automatic methods were compared in DSC, which were calculated for each of the 46 images as previously described by Zou et al. [18], where the volumetric measure of agreement was within the range of 0–1 (1 indicating the greatest overlap).

2.7. Radiomic Feature Extraction

Radiomic features from segmented MRIs were extracted via a tested and maintained open-source platform, PyRadiomics [19]. After signal intensity normalization, a total of 107 features, comprising first-order statistics, shape-based, gray-level cooccurrence matrix, gray-level run-length matrix, gray-level size zone matrix, neighboring gray-tone difference matrix, and gray-level dependence matrix, were extracted. Radiomic features were extracted from patients with known IDH1 status; 45 patients from the development set and 91 patients from test set 2 (Fig. 1).

2.8. Radiomic Feature Selection

From the development set, radiomic features were selected via Boruta, a random forest-based wrapper algorithm for all-relevant feature selection [20]. Random foresting yields an importance measure for individual features, thus minimal parameter adjustment is needed, making it popular in dimensionality-reduction tasks. Boruta algorithm was performed repeatedly to estimate feature importance, and irrelevant features were consecutively dropped. To reach statistical significance, the algorithm continuously calculated all possible feature combinations, producing an all-relevant subset of features.

2.9. Statistical Analysis

The patients' baseline clinical characteristics were analyzed using the *t*-test for age and Chi-squared or Fisher's exact test for other categorial characteristics where appropriate. Wilcoxon rank-sum tests with false discovery rate correction for multiple comparisons were used to compare the radiomic features between wild-type and mutant IDH1. Prediction of IDH1 status was based on generalized linear models (GLM) that were fitted with the relevant radiomic features. Receiver operating characteristics (ROC) curves were plotted with area under the curves (AUC) for test set 2. The optimal cut-off threshold was determined by Youden's index [21]. The 95 % CI of AUCs, sensitivities, specificities, and accuracies were estimated for each ROC analysis with 2000 stratified bootstrap samples. The statistical difference between the AUCs obtained from manual and automatic segmentations was tested via likelihood ratio test (Supplementary Materials). Statistical significance was set at $P < 0.05$. All statistical analyses were performed using R statistical software (R version 3.4.4., Vienna, Austria) and its package 'pROC' [13].

Table 2
Relevant radiomic features selected via Boruta classification.

Features	Mean importance	Median importance	Minimum importance	Maximum importance
Dependence entropy	5.519	5.622	0.131	8.619
Surface volume ratio	5.259	5.308	0.769	8.385
Run length non-uniformity	4.338	4.447	−0.255	6.801
Coarseness	4.261	4.358	−0.342	6.736
Flatness	3.951	4.030	0.103	6.758
Gray-level non-uniformity	3.514	3.589	−0.724	6.067
Run variance	3.298	3.396	−0.789	6.655
Strength	2.779	2.877	−0.765	5.836
Large area high gray-level emphasis	2.677	2.719	−0.470	5.505

IDH1 = isocitrate dehydrogenase-1, SD = standard deviation.

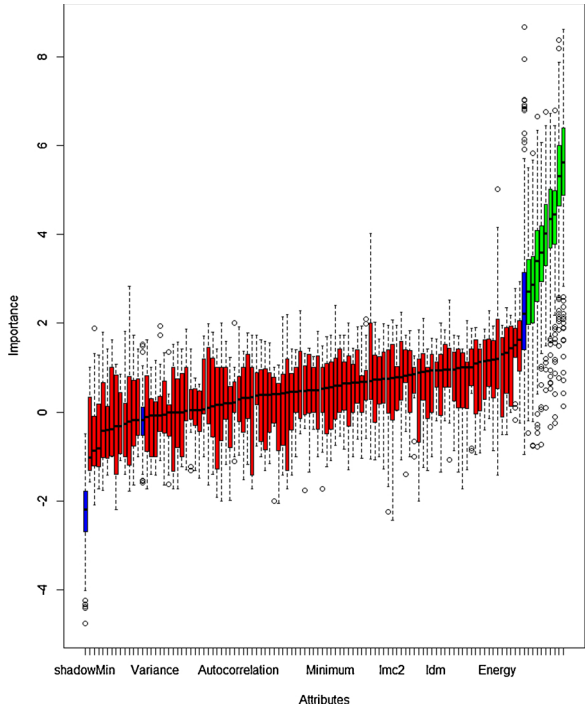

Fig. 2. Boxplots of attribute importance of radiomic features retrieved, where green and red boxplots indicate confirmed and rejected features, respectively.

3. Results

3.1. Study Population

A total of 136 patients was retrospectively included (our institution, n = 45; TCIA, n = 91) in the study. All patients had undergone pre-treatment brain MRIs. Between the two cohorts, no significant differences were found in sex, age, tumor location, and IDH1 status (Table 1). The institutional cohort had seven IDH1 mutation cases (15.6 %) whereas the TCIA cohort had eight IDH1 mutation cases (8.8 %), four of which were acquired with 1.5-T MR scanner and the other four with 3.0-T MR scanner.

3.2. Relevant Radiomic Features

A total of 107 radiomic features were extracted from both cohorts. Nine features were selected as all-relevant features by Boruta (Table 2). The selected features in the order of mean importance were: 'Dependence Entropy', 'Surface Volume Ratio', 'Run Length Non-Uniformity', 'Coarseness', 'Flatness', 'Gray-Level Non-Uniformity', 'Run Variance', 'Strength', and 'Large Area High Gray-Level Emphasis'. Fig. 2 illustrates the boxplots of attribute importance of radiomic features retrieved. Finally, compared values of nine radiomic features are summarized in Supplementary Table 2.

3.3. Dice Similarity Coefficients between Manual and Automatic Segmentations

In test set 1, the mean DSC between manual and V-Net segmentations was 0.751 ± 0.140 (range, 0.336–0.943). The representative segmentation images are depicted in Fig. 3. The DSC of individual tumors is shown in Supplementary Table 1.

3.4. Performance of IDH1 Status Prediction

The predictive performances of IDH1 status are summarized in Table 3. The AUCs were 0.904 (95 % CI: 0.81–1.0) and 0.857 (95 % CI: 0.74–0.97) for manual and V-net segmentation, respectively (Fig. 4) (P = 0.541). The optimal threshold of ROC yielded accuracy of 86.8 % (95 % CI: 63.7 %–97.8 %) and 75.8 % (95 % CI: 57.1 %–94.5 %) for manual and V-net method, respectively. There was no statistical difference between the two AUCs according to the likelihood ratio test (P = 0.073) (Supplementary Materials). The AUC of IDH1 status

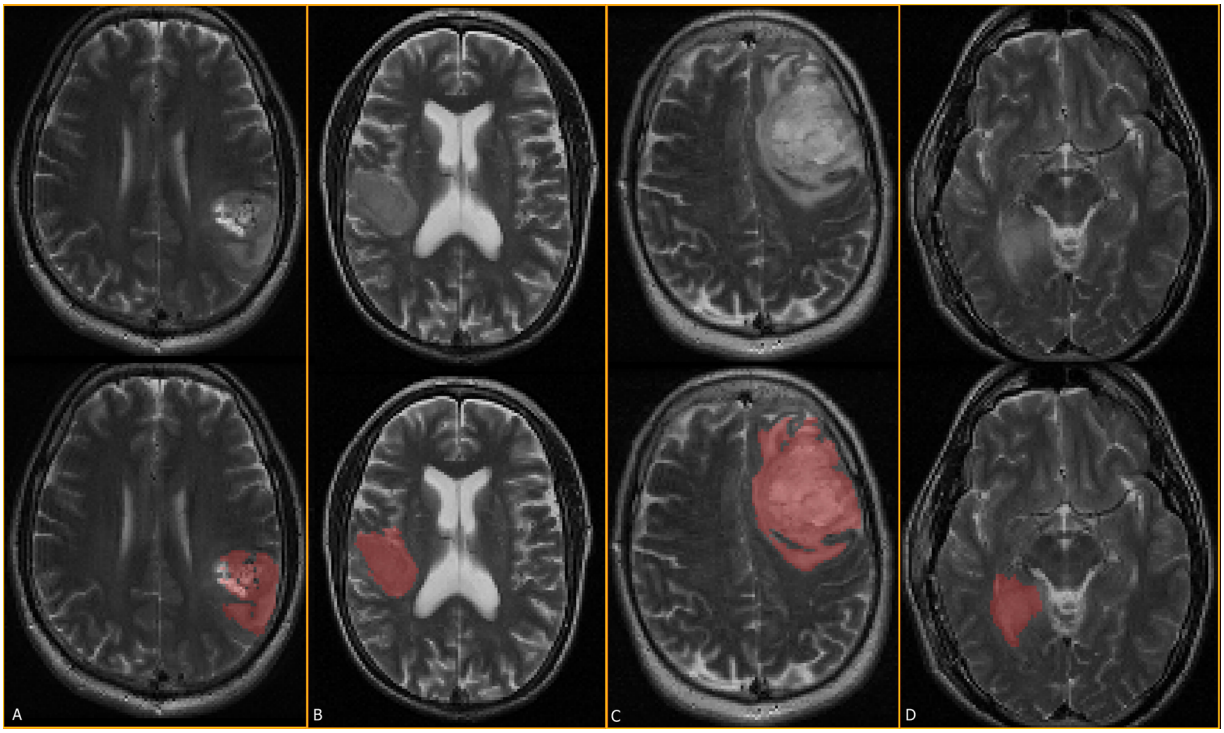

Fig. 3. Representative images of The Cancer Imaging Archive/The Cancer Genome Atlas (TCIA/TCGA) test set with unsegmented glioblastoma (upper row) and V-Net segmentation output (bottom row) in left parietal lobe (A), right frontoparietal lobe (B), left frontal lobe (C), and right temporal lobe (D).

Table 3
Comparison of IDH1 status prediction by two segmentation methods with 95 % confidence intervals.

Method	AUC[a]	Sensitivity	Specificity	Accuracy
Manual	0.904 [0.805, 1.0]	91.6 % [75, 100]	75 % [60.2, 100]	86.8 % [63.7, 97.8]
V-Net	0.857 [0.744, 0.97]	59 % [75, 100]	100 % [53.0, 96.4]	75.8 % [57.1, 94.5]

IDH1 = isocitrate dehydrogenase-1, AUC = area under the receiver operating curve.
[a] Comparison of two AUCs giving $P = 0.541$ via DeLong's test.

prediction of the development set was 0.771 (95 % CI: 0.59–0.95) with accuracy of 73.3 % (95 % CI: 46.7 %–93.3 %).

4. Discussion

Accumulating evidence suggests that IDH1 mutation status is an independent prognostic factor in patients with high-grade gliomas [22,23] having IDH1 mutations that indicate better prognoses [24]. Considering its prognostic significance, this study implemented a unique 3D image segmentation of glioblastoma on T2WI using V-Net (a fully automated volumetric CNN), which yielded reliable accuracy in predicting IDH1 mutations in glioblastoma. A previous similar study found that tumor blood flow and area of internal necrosis of enhancing tumors estimated the IDH1 mutation status with good accuracy [25]. In contrast to their study, we only applied T2WI to acquire radiomic features, achieving a comparable AUC without a complex parameter, such as arterial spin labeling. The benefit of implementing only T2WI is its generalizability, as it is the most commonly acquired brain MR sequence. At the same time, T2WI was reported to reflect heterogeneity of glioblastoma and was capable of differentiating it from pseudo-progression [26]. The results of current study are also consistent with another similar study by Lee et al. [27], who implemented radiomic analysis to predict IDH1 mutation status in glioblastoma. While our IDH1 predictive performance was similar to their study (Lee et al.: 70.3–87.3 % prediction rate vs. current study: 75.8–86.8 %), they used only manual segmentation of multi-parametric MRI.

The segmentation performance of V-Net in our study was similar to other similar segmentation approaches. Isensee et al. used a CNN-based algorithm to segment brain tumors and achieved DSC of 0.647 − 0.858 for different subregions of tumors [13]. The distinctive strength of this study lies in its fully automatic 3D image segmentation. This is important since segmentation is a crucial step prior to further image analysis of tumors in any organ. Most previous studies performing similar image analyses used time-consuming manual delineation of ROI [25,27,28], which is often susceptible to errors and inter-rater variabilities. The results of this study showed that reliable segmentation capabilities could be achieved after training the V-net with a small number of samples (n = 45). Additionally, the possibility of overfitting, which is common in machine-learning algorithms, was minimized by training the V-Net model solely from the development set and testing it using an external test set. Furthermore, only T2WI, the most commonly acquired conventional sequence, was used throughout the analysis and segmentation of multi-parametric sequences such as gadolinium-enhanced T1-weighted, diffusion-weighted, and perfusion-weighted images was not needed, simplifying the time-consuming pre-processing and computational time. One of the significant progresses made in the field of noninvasively estimating IDH1 mutation status is based on measuring 2-hydroxyglutarate (2 H G) using MR spectroscopy. Several studies have reliably estimated IDH1 status via this method; however, varying accuracies and false-positive rates were reported due to factors such as tumor volume [29], cutoff values [30], proportion of necrosis, and apparent diffusion coefficients [31]. Considering radiomics have limited reproducibility across different settings, it is important to note that both 2 H G and radiomics are under technical development and are yet to be incorporated into routine clinical practice.

It is interesting that some of the selected features overlap with a similar previous study by Yu et al. [32]. For example, features such as 'Surface Volume Ratio', 'Run Variance', and 'Large Area High Gray-Level Emphasis' were also found to be meaningful features in discriminating IDH1 mutation status. Of importance, the median value of 'Surface Volume Ratio' was found to be lower in IDH1 mutant glioblastomas; considering lower 'Surface Volume Ratio' indicates more compact and spherical shape, sphericity might be associated with IDH1 mutant glioblastoma. Although their study cohort consisted of grade II

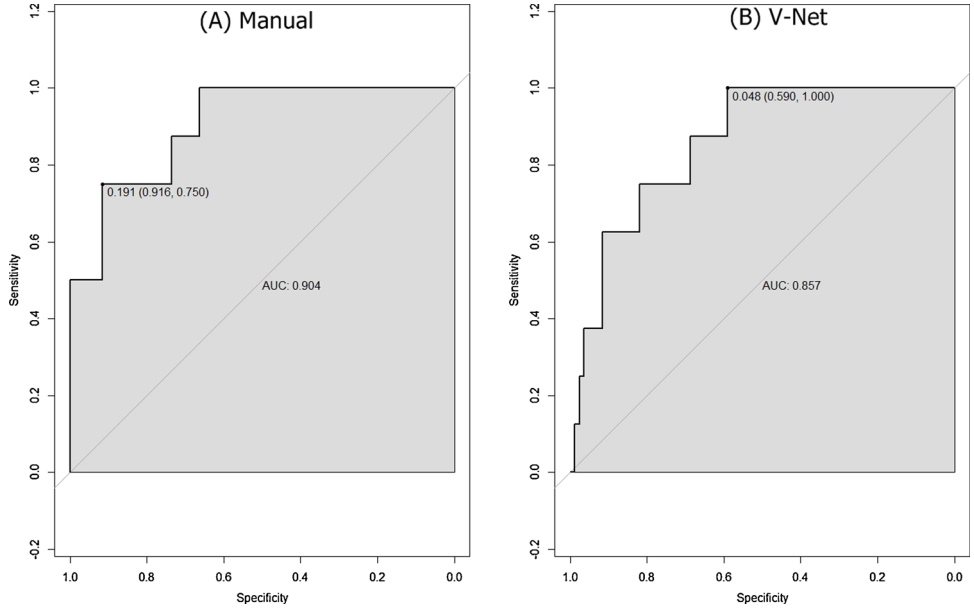

Fig. 4. Receiver operating characteristics (ROC) curves of IDH1 mutation predicted by radiomic features from (A) manual and (B) V-Net segmentation.

gliomas, these overlapping features might have discriminative ability in predicting IDH1 status in both low and high-grade gliomas.

There are a few limitations in this study, apart from the potential selection bias associated with the retrospective study design. Due to the inherent rarity of IDH1 mutations in glioblastoma, creating a separate internal validation set was not possible. Instead, application of V-Net algorithm on a separate test set (i.e. not used in training the model) would have minimized potential overfitting. Moreover, IDH2 mutations (a minority of such mutations was accounted for) were not included due to lack of available data. Additionally, even though images from two different sites were analyzed, minimal pre-processings (intensity normalization and spatial interpolation, which could be fully automated) were performed. Nonetheless, considering only one sequence (T2WI) was used throughout the study, no co-registration and pre-processing were needed. Finally, a few automatic segmentations demonstrated poor performances (i.e. low DSC) compared to the reference manual segmentation. The erroneous segmentations included cerebrospinal fluid of lateral ventricles, which seemed to occur when extensive T2 hyperintense peritumoral edema were near the lateral ventricles. This suggests a room for further refinement of the model.

In conclusion, the current study applied V-net to automatically segment glioblastoma on T2WI from which radiomic features were extracted to predict IDH1 mutation. Compared to the manual segmentation, radiomic analysis from automatic segmentation yielded reliable capability in predicting IDH1 mutation status. Future studies are needed to explore application of V-Net onto multi-parametric MRI with sub-regional segmentations.

CRediT authorship contribution statement

Yangsean Choi: Conceptualization, Methodology, Validation, Formal analysis, Investigation, Data curation, Writing - original draft, Visualization. **Yoonho Nam:** Methodology, Software, Validation, Writing - review & editing. **Youn Soo Lee:** Resources. **Jiwoong Kim:** Methodology, Formal analysis, Writing - review & editing. **Kook-Jin Ahn:** Resources, Writing - review & editing, Supervision. **Jinhee Jang:** Resources, Supervision. **Na-Young Shin:** Resources, Supervision. **Bum-Soo Kim:** Resources, Supervision. **Sin-Soo Jeon:** Resources.

Declaration of Competing Interest

The authors declare that they have no conflict of interest.

Acknowledgements

This research did not receive any specific grant from funding agencies in the public, commercial, or not-for-profit sectors.

Appendix A. Supplementary data

Supplementary material related to this article can be found, in the online version, at doi:https://doi.org/10.1016/j.ejrad.2020.109031.

References

[1] R. Stupp, W.P. Mason, M.J. van den Bent, M. Weller, B. Fisher, M.J. Taphoorn, K. Belanger, A.A. Brandes, C. Marosi, U. Bogdahn, J. Curschmann, R.C. Janzer, S.K. Ludwin, T. Gorlia, A. Allgeier, D. Lacombe, J.G. Cairncross, E. Eisenhauer, R.O. Mirimanoff, Radiotherapy plus concomitant and adjuvant temozolomide for glioblastoma, N. Engl. J. Med. 352 (10) (2005) 987–996.

[2] H. Yan, D.W. Parsons, G. Jin, R. McLendon, B.A. Rasheed, W. Yuan, I. Kos, I. Batinic-Haberle, S. Jones, G.J. Riggins, IDH1 and IDH2 mutations in gliomas, N. Engl. J. Med. 360 (8) (2009) 765–773.

[3] C. Hartmann, B. Hentschel, W. Wick, D. Capper, J. Felsberg, M. Simon, M. Westphal, G. Schackert, R. Meyermann, T. Pietsch, G. Reifenberger, M. Weller, M. Loeffler, A. von Deimling, Patients with IDH1 wild type anaplastic astrocytomas exhibit worse prognosis than IDH1-mutated glioblastomas, and IDH1 mutation status accounts for the unfavorable prognostic effect of higher age: implications for classification of gliomas, Acta Neuropathol. 120 (6) (2010) 707–718.

[4] M. Sanson, Y. Marie, S. Paris, A. Idbaih, J. Laffaire, F. Ducray, S.E. Hallani, B. Boisselier, K. Mokhtari, K. Hoang-Xuan, J.-Y. Delattre, Isocitrate dehydrogenase 1 codon 132 mutation is an important prognostic biomarker in gliomas, J. Clin. Oncol. 27 (25) (2009) 4150–4154.

[5] H. Tang, M. Moradi, A.E. Harouni, H. Wang, G. Veni, P. Prasanna, T. Syeda-Mahmood, Segmentation of anatomical structures in cardiac CTA using multi-label V-Net, SPIE2018 (2018).

[6] E. Gibson, F. Giganti, Y. Hu, E. Bonmati, S. Bandula, K. Gurusamy, B. Davidson, S.P. Pereira, M.J. Clarkson, D.C. Barratt, Automatic multi-organ segmentation on abdominal CT with dense V-Networks, IEEE Trans. Med. Imaging 37 (8) (2018) 1822–1834.

[7] P.F. Christ, F. Ettlinger, F. Grün, M.E.A. Elshaera, J. Lipkova, S. Schlecht, F. Ahmaddy, S. Tatavarty, M. Bickel, P. Bilic, Automatic Liver and Tumor Segmentation of CT and MRI Volumes Using Cascaded Fully Convolutional Neural Networks, preprint arXiv:1702.05970 arXiv, 2017.

[8] G. Zeng, X. Yang, J. Li, L. Yu, P.-A. Heng, G. Zheng, 3D U-Net with Multi-Level Deep Supervision: Fully Automatic Segmentation of Proximal Femur in 3D MR Images, Springer International Publishing, Cham, 2017, pp. 274–282.

[9] Z. Tian, L. Liu, Z. Zhang, B. Fei, PSNet: prostate segmentation on MRI based on a convolutional neural network, J. Med. Imaging 5 (2) (2018) 021208.

[10] Q. Zhu, B. Du, B. Turkbey, P. Choyke, P. Yan, Exploiting interslice correlation for MRI prostate image segmentation, from recursive neural networks aspect, Complexity 2018 (2018).

[11] B. Wang, Y. Lei, S. Tian, T. Wang, Y. Liu, P. Patel, A.B. Jani, H. Mao, W.J. Curran, T. Liu, Deeply supervised 3D fully convolutional networks with group dilated convolution for automatic MRI prostate segmentation, Med. Phys. 46 (4) (2019) 1707–1718, https://doi.org/10.1002/mp.13416.

[12] A. Casamitjana, M. Catà, I. Sánchez, M. Combalia, V. Vilaplana, Cascaded V-Net using ROI masks for brain tumor segmentation, International MICCAI Brainlesion Workshop (2017) 381–391.

[13] F. Isensee, P. Kickingereder, W. Wick, M. Bendszus, K.H. Maier-Hein, Brain Tumor Segmentation and Radiomics Survival Prediction: Contribution to the BRATS 2017 Challenge, Springer International Publishing, Cham, 2018, pp. 287–297.

[14] F. Milletari, N. Navab, S.-A. Ahmadi, V-Net: fully convolutional neural networks for volumetric medical image segmentation, 2016 Fourth International Conference on 3D Vision (3DV) (2016) 565–571.

[15] K. Clark, B. Vendt, K. Smith, J. Freymann, J. Kirby, P. Koppel, S. Moore, S. Phillips, D. Maffitt, M. Pringle, L. Tarbox, F. Prior, The cancer imaging archive (TCIA): maintaining and operating a public information repository, J. Digit. Imaging 26 (6) (2013) 1045–1057.

[16] A. Fedorov, R. Beichel, J. Kalpathy-Cramer, J. Finet, J.-C. Fillion-Robin, S. Pujol, C. Bauer, D. Jennings, F. Fennessy, M. Sonka, J. Buatti, S. Aylward, J.V. Miller, S. Pieper, R. Kikinis, 3D Slicer as an image computing platform for the Quantitative Imaging Network, Magn. Reson. Imaging 30 (9) (2012) 1323–1341.

[17] O. Ronneberger, P. Fischer, T. Brox, U-Net: convolutional networks for biomedical image segmentation, International Conference on Medical Image Computing and Computer-Assisted Intervention (2015) 234–241.

[18] K.H. Zou, S.K. Warfield, A. Bharatha, C.M. Tempany, M.R. Kaus, S.J. Haker, W.M. Wells 3rd, F.A. Jolesz, R. Kikinis, Statistical validation of image segmentation quality based on a spatial overlap index, Acad. Radiol. 11 (2) (2004) 178–189.

[19] J.J. Van Griethuysen, A. Fedorov, C. Parmar, A. Hosny, N. Aucoin, V. Narayan, R.G. Beets-Tan, J.-C. Fillion-Robin, S. Pieper, H.J. Aerts, Computational radiomics system to decode the radiographic phenotype, Cancer Res. 77 (21) (2017) e104–e107.

[20] M.B. Kursa, W.R. Rudnicki, Feature selection with the boruta package, J. Stat. Softw. 36 (11) (2010) 1–13.

[21] J. Zhang, D.P. Barboriak, H. Hobbs, M.A. Mazurowski, A fully automatic extraction of magnetic resonance image features in glioblastoma patients, Med. Phys. 41 (4) (2014) 042301.

[22] K. Ichimura, D.M. Pearson, S. Kocialkowski, L.M. Bäcklund, R. Chan, D.T.W. Jones, V.P. Collins, IDH1 mutations are present in the majority of common adult gliomas but rare in primary glioblastomas, Neuro Oncol. 11 (4) (2009) 341–347.

[23] J.K. Myung, H.J. Cho, C.K. Park, S.K. Kim, J.H. Phi, S.H. Park, IDH1 mutation of gliomas with long-term survival analysis, Oncol. Rep. 28 (5) (2012) 1639–1644.

[24] S. Nobusawa, T. Watanabe, P. Kleihues, H. Ohgaki, IDH1 mutations as molecular signature and predictive factor of secondary glioblastomas, Clin. Cancer Res. 15 (19) (2009) 6002–6007.

[25] K. Yamashita, A. Hiwatashi, O. Togao, K. Kikuchi, R. Hatae, K. Yoshimoto, M. Mizoguchi, S.O. Suzuki, T. Yoshiura, H. Honda, MR imaging-based analysis of glioblastoma multiforme: estimation of IDH1 mutation status, AJNR Am. J. Neuroradiol. 37 (1) (2016) 58–65.

[26] T.C. Booth, T.J. Larkin, Y. Yuan, M.I. Kettunen, S.N. Dawson, D. Scoffings, H.C. Canuto, S.L. Vowler, H. Kirschenlohr, M.P. Hobson, Analysis of heterogeneity in T2-weighted MR images can differentiate pseudoprogression from progression in glioblastoma, PLoS One 12 (5) (2017) e0176528.

[27] M.H. Lee, J. Kim, S.T. Kim, H.M. Shin, H.J. You, J.W. Choi, H.J. Seol, D.H. Nam, J.I. Lee, D.S. Kong, Prediction of IDH1 mutation status in the glioblastoma using the machine learning technique based on the quantitative radiomic data, World Neurosurg. 125 (2019) e688–e696.

[28] J. Lee, S.H. Choi, J.H. Kim, C.H. Sohn, S. Lee, J. Jeong, Glioma grading using apparent diffusion coefficient map: application of histogram analysis based on automatic segmentation, NMR Biomed. 27 (9) (2014) 1046–1052.

[29] M.I. de la Fuente, R.J. Young, J. Rubel, M. Rosenblum, J. Tisnado, S. Briggs, J. Arevalo-Perez, J.R. Cross, C. Campos, K. Straley, D. Zhu, C. Dong, A. Thomas, A.A. Omuro, C.P. Nolan, E. Pentsova, T.J. Kaley, J.H. Oh, R. Noeske, E. Maher,

C. Choi, P.H. Gutin, A.I. Holodny, K. Yen, L.M. DeAngelis, I.K. Mellinghoff, S.B. Thakur, Integration of 2-hydroxyglutarate-proton magnetic resonance spectroscopy into clinical practice for disease monitoring in isocitrate dehydrogenase-mutant glioma, Neuro Oncol. 18 (2) (2016) 283–290.

[30] G. Lombardi, G. Corona, L. Bellu, A. Della Puppa, A. Pambuku, P. Fiduccia, R. Bertorelle, M.P. Gardiman, D. D'Avella, G. Toffoli, V. Zagonel, Diagnostic value of plasma and urinary 2-hydroxyglutarate to identify patients with isocitrate dehydrogenase-mutated glioma, Oncologist 20 (5) (2015) 562–567.

[31] C.H. Suh, H.S. Kim, W. Paik, C. Choi, K.H. Ryu, D. Kim, D.-C. Woo, J.E. Park, S.C. Jung, C.G. Choi, S.J. Kim, False-positive measurement at 2-hydroxyglutarate MR spectroscopy in isocitrate dehydrogenase wild-type glioblastoma: a multifactorial analysis, Radiology 291 (3) (2019) 752–762.

[32] J. Yu, Z. Shi, Y. Lian, Z. Li, T. Liu, Y. Gao, Y. Wang, L. Chen, Y. Mao, Noninvasive IDH1 mutation estimation based on a quantitative radiomics approach for grade II glioma, Eur. Radiol. 27 (8) (2017) 3509–3522.